# Formation of antihydrogen in an antiproton-positron Debye plasma in the presence of an external laser field

Sougata Mukhopadhyay and C. Sinha
*Department of Theoretical Physics, Indian Association for the Cultivation of Science, Jadavpur, Kolkata-700032, India*
(Received 29 July 2013; published 11 September 2013)

We study quantum mechanically the influence of an external laser field on the antihydrogen ($\bar{H}$) formation cross sections in ground and excited states ($2s$,$2p$) via the three-body recombination process inside a dense plasma of antiprotons and positrons, supposed to be the most efficient mechanism for cold and trapped antihydrogen. The plasma screening is considered in the framework of a Debye- Hückel potential. The laser polarization is chosen to be parallel to the incident momentum of the passive positron. The modifications due to the presence of the laser field are found to be quite significant both quantitatively and qualitatively for all the states. In the presence of a laser, the $\bar{H}$ formation cross sections are found to be suppressed significantly with respect to the field-free situation particularly in the ground state, while the excited state cross sections are in general enhanced at very low incident energies but are again suppressed at higher energies except for some special cases. The sensitivity of the formation cross sections with respect to the Debye length are also studied both in the laser-assisted and in the field-free situations. At very low incident energies, the ground state multiphoton formation is found to enhance with the increase in Debye screening, while the reverse is true for the excited states. These findings should have important implications for future $\bar{H}$ studies.

DOI: 10.1103/PhysRevA.88.033414 PACS number(s): 34.80.Qb, 34.80.Lx, 52.20.Hv

## I. INTRODUCTION

Currently, the production of cold and trapped antihydrogen ($\bar{H}$), the simplest and the most stable bound state of antimatter, is one of the most promising topics from the theoretical and experimental points of view mainly because, by precise comparisons between hydrogen and antihydrogen, one can study various fundamental symmetries between matter and antimatter. The major challenge facing the $\bar{H}$ research is the production of a significant amount of cold and trapped ground state $\bar{H}$, which is an ideal system for performing the long awaited high precision spectroscopic studies as well as gravitational studies to test the *CPT* invariance of the standard model of fundamental particles and interactions as well as the gravitational weak equivalence principle (WEP) of antimatter. Any violation of these symmetries would require new physics beyond the standard model which demands that H and $\bar{H}$ have the same spectrum. Apart from these, there are many important practical applications of $\bar{H}$, e.g., for igniting inertial confinement fusion pellets, in the propulsion system, in cancer therapy, etc.

The recent technological advances in the cooling and trapping mechanisms of antiprotons ($\bar{p}$) and positrons ($e^+$) have now made it feasible to produce an increasing amount of cold and trapped $\bar{H}$ at the laboratories [1–30]. This has motivated theoretical workers to venture and study different processes for the formation of antihydrogen. Among all the processes leading to the formation of $\bar{H}$ [3], the most efficient mechanism for the production of cold $\bar{H}$ is the three-body recombination (TBR) using cold antiproton and positron plasmas [1–46]

$$\bar{p} + e^+ + e^+ \rightarrow \bar{H} + e^+ \qquad (1)$$

in which a spectator particle ($e^+$) carries away the excess energy and the momentum released in the recombination. At low incident energies, the $\bar{H}$ produced via the TBR process is found to be several orders of magnitude larger [5,6,9,10,13–15,33,35] as compared to other $\bar{H}$ formation processes, e.g., the radiative recombination of $e^+$ and $\bar{p}$ [33,37] and the three-body charge transfer between the positronium (Ps) and the $\bar{p}$ [33,38–45]. Earlier the TBR reaction (1) was studied theoretically [31–34] in a plasma environment at low temperatures in the framework of classical Monte Carlo simulations. For a weakly correlated plasma, Glinsky and O'Neil [31] deduced classically the scaling law for the TBR rate ($R_3$) as $R_3 \sim T^{-9/2}$. However, such simple power-law scaling could not be found in the $\bar{H}$ experiments [5(b)], although at comparatively higher incident energies than those in the experiments at CERN, quantum-mechanical calculations [36] for the TBR process corroborated this scaling behavior for certain parameters.

Since in most of the recent collision experiments, laser field is used for different technological purposes, e.g., for cooling and trapping as well as for collimation, it is highly desirable to study the aforesaid TBR process in the presence of an external laser field. In particular, the experiments at CERN by different groups—ATRAP [7–9], ATHENA [10], and later on by ALPHA [17]—on the production of cold and trapped $\bar{H}$, used lasers for different technological purposes, e.g., controlling the reactions (laser induced), laser cooling, etc. As such, theoretically it becomes necessary to study the influence of an external laser field on the TBR process (1) producing $\bar{H}$.

Furthermore, in recent years much attention is being paid to the study of different atomic processes embedded in a plasma [47–66]. This is mainly because in most of the collision experiments with or without the presence of a laser, the plasma environment is always present to some extent and it can significantly affect the collision processes. In particular, the recent experiments [19–30] on cold $\bar{H}$ formations were performed in the TBR process (1) using cold and trapped positron and antiproton plasmas. It is therefore highly desirable and quite worthwhile to study the aforesaid TBR process

 

in the combined presence of plasma and an external laser field. The present study addresses this, where the constituents of the laser-assisted TBR reaction forming $\bar{\mathrm{H}}$ are embedded in plasma.

Now, inside a dense plasma, partial shielding by the neighboring charged particles weakens the pure Coulomb interaction between two charged particles at large separations, thereby affecting the collision properties, e.g., collision strength, collision cross section, etc. However, not much is known about the combined effects of plasma and laser field on important collision processes and only a limited number of studies [47,53,65] were made along this line.

When a dense plasma is irradiated with an external laser field, the electromagnetic wave will not propagate through the plasma in the nonrelativistic case, if the plasma frequency is much higher than the frequency of the electromagnetic wave. However, there will still be a transfer of energy from the laser to the plasma without altering the average plasma properties [67].

In the present work, we have proposed a quantum-mechanical approach for the formation of $\bar{\mathrm{H}}$ in the ground $(1s)$ and excited $(2s,2p)$ states via the laser-assisted TBR process (1) in a plasma of antiprotons and positrons. Inside the plasma, the interactions between the charged particles and the ions are screened and the screened potential is considered in the framework of the Debye-Hückel approximation [68]. The effective screened Coulomb potential is known in plasma physics as the Debye-Hückel potential and is given by $V(r) = -e^{-\mu r}/r$ ( $-$ sign for attractive case), where $\mu$ is called the Debye screening parameter and is given by $\mu = 1/\Lambda = [4\pi n(Ze)^2/k_BT]^{0.5}$, where $n$ is the plasma density, $T$ is the temperature of the plasma, and $\Lambda$ is the Debye length. A smaller value of $\Lambda$ can be associated with stronger screening. This screened Coulomb potential effectively reduces the binding energy and pushes the system towards gradual instability with the increase of screening [59].

We consider an ensemble of weakly correlated positron $(e^+)$ plasma and the density of the plasma is assumed to be low enough so that the $e^+$-$e^+$ interaction in the initial channel can be treated as a perturbation. In other words for such a weakly coupled plasma, the average Coulomb energy is much less than the average kinetic energy [69]. Further, the effect of the exchange between the active and the spectator $e^+$'s is quite dominant in this process and the present model incorporates this in a consistent manner. The energy range considered here is relatively much higher (∼1–100 eV) as compared to the extreme low energy (∼meV range) experiments at CERN [1–30] for which the present model is not expected to be adequate. Both the differential (DCS) as well as the total (TCS) $\bar{\mathrm{H}}$ formation cross sections in the ground and excited states $(n = 2)$ are studied in the field-free (FF) as well as in the laser-assisted (LA) situations.

## II. THEORY

The present work deals with the following LA TBR process in the ground and excited states:

$$\bar{p} + e^+ + e^+ + N\gamma(\omega,\vec{\varepsilon}) \rightarrow \bar{\mathrm{H}}(\bar{\mathrm{H}}^*) + e^+, \tag{2}$$

where $N$ stands for the multiphoton absorption and emission and $\gamma(\omega,\vec{\varepsilon})$ denotes the laser photon with angular frequency $\omega$ and field strength $\vec{\varepsilon}_0$. The laser field (cw) is treated classically and is chosen to be a single-mode, linearly polarized, spatially homogeneous electric field presented by $\vec{\varepsilon}(t) = \vec{\varepsilon}_0 \sin(\omega t + \xi)$, where $\xi$ is the initial phase of the laser field, the corresponding vector potential in the Coulomb gauge is $\vec{A}(t) = \vec{A}_0 \cos\omega t$ with $\vec{A}_0 = \vec{\varepsilon}_0/\omega$, and $\xi$ is chosen to be zero in the present work.

The prior form of the transition matrix element for the laser-assisted TBR process (2) is given by

$$T_{if} = -i\int_{-\infty}^{\infty} dt\,\langle\Psi_f^-(\vec{r}_1,\vec{r}_2)(1+\vec{P})|V_i|\psi_i(\vec{r}_1,\vec{r}_2)\rangle, \tag{3}$$

where $\vec{P}$ denotes the exchange operator corresponding to the interchange of the two positrons in the final channel and $V_i$ is the initial channel perturbation. We have used atomic units $\hbar = m = e = 1$ throughout the calculations.

The total Hamiltonian $(H)$ of the system may be written as

$$H = -\tfrac{1}{2}(i\vec{\nabla}_1 + \vec{A})^2 - \tfrac{1}{2}(i\vec{\nabla}_2 + \vec{A})^2 + V_i, \tag{4}$$

where $V_i$ represents the Debye-Hückel potential [68] felt by the positrons in the initial channel inside the plasma and is of the form

$$V_i = -\frac{2Z}{r_1}e^{-\mu r_1} - \frac{2Z}{r_2}e^{-\mu r_2} + \frac{2}{r_{12}}e^{-\mu r_{12}}. \tag{5}$$

$\vec{r}_1$ and $\vec{r}_2$ represent the position vectors of the active $e^+(\vec{r}_1)$ and the spectator $e^+(\vec{r}_2)$ with respect to the fixed antiproton and $r_{12}$ is the relative distance between the two positrons. Equation (5) indicates that the plasma changes the potential of free space causing its attenuation with a decay length equal to the Debye length $\Lambda$. This screening of the potential produced by a local charge in the plasma is the Debye shielding effect [68].

The energy conservation relation for the TBR process (2) is given by

$$\frac{k_1^2}{2} + \frac{k_2^2}{2} \pm N\omega = \frac{k_f^2}{2} + \varepsilon_{\bar{\mathrm{H}}}, \tag{6}$$

where $\vec{k}_1$ and $\vec{k}_2$ are the incident momentum of the active and the spectator positrons $(e^+s)$, respectively, where $\vec{k}_f$ is the final momentum of the outgoing spectator $e^+$, $\varepsilon_{\bar{\mathrm{H}}}$ is the binding energy of $\bar{\mathrm{H}}$, $N$ is the number of photon exchange, "$+N$" refers to absorption, and "$-N$" refers to the emission of photons.

The initial channel asymptotic wave function $\psi_i$ in Eq. (3), dressed by the laser field satisfies the following Schrödinger equation:

$$\left[-\tfrac{1}{2}(i\vec{\nabla}_1 + \vec{A})^2 - \tfrac{1}{2}(i\vec{\nabla}_2 + \vec{A})^2 - E\right]\psi_i = 0 \tag{7}$$

and is given by

$$\psi_i = \chi_{k_1}\chi_{k_2}, \tag{8}$$

where $\chi_{k_i}$; $i = 1,2$ refers to the Volkov solution [70] corresponding to the two incident positrons (1,2) and $\vec{k}_1$,$\vec{k}_2$ are the incident momenta of the active (1) and the spectator (2) positrons, respectively,

$$\chi_{k_i} = e^{i(\vec{k}_i\cdot\vec{r}_i + \vec{k}_i\cdot\vec{\alpha}_0\sin\omega t - E_{k_i}t)} \tag{9}$$

with $\vec{\alpha}_0 = \vec{\varepsilon}_0/\omega^2$ and $\vec{k}_i$ stands for the momentum of the active $(\vec{k}_1)$ or the spectator $e^+$ $(\vec{k}_2)$. The effect of the laser field on

the antiproton in the initial channel is neglected. This is quite legitimate on account of the heavy mass of the antiproton as compared to the positrons.

The final channel wave function $\Psi_f^-$ in Eq. (3) satisfies the three-body Schrödinger equation obeying the incoming wave boundary condition:

$$(H - E)\Psi_f^- = 0. \tag{10}$$

The exact solution of Eq. (10) does not exist and in the present model $\Psi_f^-$ is approximated in the framework of eikonal approximation as follows:

$$\Psi_f^- = \chi_{k_f}(\vec{r}_2,t)\phi_{\bar{\mathrm{H}}}^d(\vec{r}_1,t), \tag{11}$$

where $\chi_{k_f}(\vec{r}_2,t)$ represents the eikonal modified dressed Volkov state of the outgoing scattered positron (spectator) given by

$$\chi_{k_f} = \exp\, i(\vec{k}_f\cdot\vec{r}_2 + \vec{k}_f\cdot\vec{\alpha}_0 \sin\,\omega t - E_{k_f}t) \exp\left[i\eta_f\int_z^\infty\left(\frac{1}{r_{12}}-\frac{1}{r_2}\right)dz\prime\right] \tag{12}$$

with $\vec{\alpha}_0 = \vec{\varepsilon}_0/\omega^2$, $\eta_f = 1/|\vec{k}_f - \vec{A}(t)|$, and $\vec{k}_f$ is the final momentum of the spectator positron.

The eikonal phase term (laser modified) in Eq. (12) accounts for the interaction (higher order effect) between the outgoing passive positron and the $\bar{\mathrm{H}}$ in the final channel.

The laser dressed ground state wave function of the $\bar{\mathrm{H}}$ in the final channel is constructed by solving the Schrödinger equation in the framework of first order perturbation theory using the Coulomb gauge and is given by

$$\phi_{\bar{\mathrm{H}}}^d(\vec{r}_1,t) = \frac{1}{\sqrt{\pi}}e^{-iW_0^{\bar{\mathrm{H}}}t}e^{-\lambda_f r_1}[1 + i\vec{A}(t)\cdot\vec{r}_1], \tag{13}$$

where $W_0^{\bar{\mathrm{H}}}$ is the energy of the ground state $\bar{\mathrm{H}}$.

In the presence of the laser field, the angular momentum $l$ is no longer a good quantum number and as such the excited states $(2s,2p)$ lose their identity in presence of the field. In fact, since the dipole operator has a nonvanishing matrix element between the $2s$ and $2p_0$ states, these two states are mixed by the dipole perturbation and as such the dressed $\bar{\mathrm{H}}$ formed in the excited state ($2s$ or $2p$) could be expressed as a superposition of the $2s$ and $2p_0$ states (linear combination) as follows:

$$\phi_{\bar{\mathrm{H}}}^d(\vec{r}_1,t) = \frac{1}{\sqrt{2}}\left[\psi_1(r_1)e^{-i/\hbar(E_{n=2}-\Delta E)t} \pm \psi_2(r_1)e^{-i/\hbar(E_{n=2}+\Delta E)t}\right], \tag{14a}$$

where $\Delta E = \pm 3e\varepsilon/Z$ denotes the Stark shift in a.u. where $e$ is the charge of the bound $e/e^+$, being $-1$ for electron and $+1$ for positron. $Z$ is the charge of the target atom.

$$\psi_1 = \frac{1}{\sqrt{2}}(\psi_{200} + \psi_{210}) \quad \text{and} \quad \psi_2 = \frac{1}{\sqrt{2}}(\psi_{200} - \psi_{210}). \tag{14b}$$

In Eq. (14b) $\psi_1$ represents the lower energy state, while $\psi_2$ represents the upper energy state.

We henceforth designate the lower energy state as $2s$ and the upper energy state as $2p$. It may be mentioned here that since the laser field is always chosen along the direction of the polar axis, only the $m = 0$ state contributes to this laser-assisted process since by the dipole selection rule $\Delta m = 0$.

In view of Eqs. (3), (5), (8), (9), and (11), the space part of the transition matrix element $T_{if}$ in (3) can be carried out to obtain

$$I = -\int \exp(i\vec{k}_1\cdot\vec{r}_1)\exp(i\vec{k}_2\cdot\vec{r}_2)\left(\frac{r_2+z_{2z}}{r_{12}+z_{12}}\right)^{-i\eta_f} \times V_i e^{-\lambda_{\mathrm{H}}r_1}e^{-i\vec{k}_{2f}\cdot\vec{r}_2}d\vec{r}_1\,d\vec{r}_2. \tag{15}$$

Now, in order to carry out the time integration in Eq. (3), we recast the eikonal modified Volkov state of the positron in Eq. (12) in the following manner:

$$\chi_{k_f} = (2\pi)^{-3/2}\sum_{m=-\infty}^{\infty}(-i)^m J_m(\vec{k}_f\cdot\alpha_0) \times \exp\{i[\vec{k}_f\cdot\vec{r}_2 - (E_f - m\omega)t]\}\left(\frac{r_2+z_{2z}}{r_{12}+z_{12}}\right)^{-i\eta_f}. \tag{16}$$

Finally, after performing the time integration [71] in Eq. (3), the transition matrix element $T_{if}$ reduces to

$$T_{if} = -i\frac{1}{(2\pi)^{1/2}}\sum_N \delta(E_{k_f} - E_{k_1} - E_{k_2} + N\omega)J_N(\vec{K}\cdot\vec{\alpha}_0)I, \tag{17a}$$

where $J_N$ is the Bessel function of order $N$, $\vec{K} = \vec{k}_1 + \vec{k}_2 - \vec{k}_f$, and the integral $I$ being the space part of the transition matrix element. In deducing Eq. (17a) we make use of the following generating function of the Bessel function:

$$e^{ix\,\sin\,y} = \sum_{N=-\infty}^{\infty} J_N(x)e^{iNy}. \tag{17b}$$

It should be noted that in performing the time integration analytically we approximate the quantity $\vec{A}(t)$ in the eikonal phase term in Eq. (12) by its initial $t = 0$ value ($\vec{A}_0$).

Finally the laser-assisted differential cross section $(d\sigma/d\Omega)$ for the formation of $\bar{\mathrm{H}}$ for $N$ photon transfer is given as

$$\left(\frac{d\sigma}{d\Omega}\right)_N = \frac{k_f}{k_1k_2}[T_{if}]^2 = \frac{k_f}{k_1k_2}\left[\frac{1}{4}|f+g|^2 + \frac{3}{4}|f-g|^2\right], \tag{18}$$

where $f$ and $g$ are the direct and exchange amplitudes, respectively.

The total laser-assisted differential cross section $(d\sigma/d\Omega)$ is the sum over all multiphoton processes, i.e., $(d\sigma/d\Omega) = \sum_{N=-\infty}^{\infty}(d\sigma/d\Omega)_N$.

The TCS for a given value of $N$ can be obtained by integrating the differential cross section in Eq. (18) over the solid angle,

$$\sigma_N = \int\left(\frac{d\sigma}{d\Omega}\right)_N d\Omega. \tag{19}$$

and the total multiphoton cross section is given by

$$\sigma = \sum_N \sigma_N. \tag{20}$$

### III. RESULTS AND DISCUSSIONS

We have computed the DCS and the TCS in the FF as well as in the LA situations for the plasma (Debye) embedded three-body recombination reaction (2) leading to the formation of $\bar{H}$ in the ground ($1s$) state and excited ($2s$,$2p$) states taking account of the exchange effect between the active and the

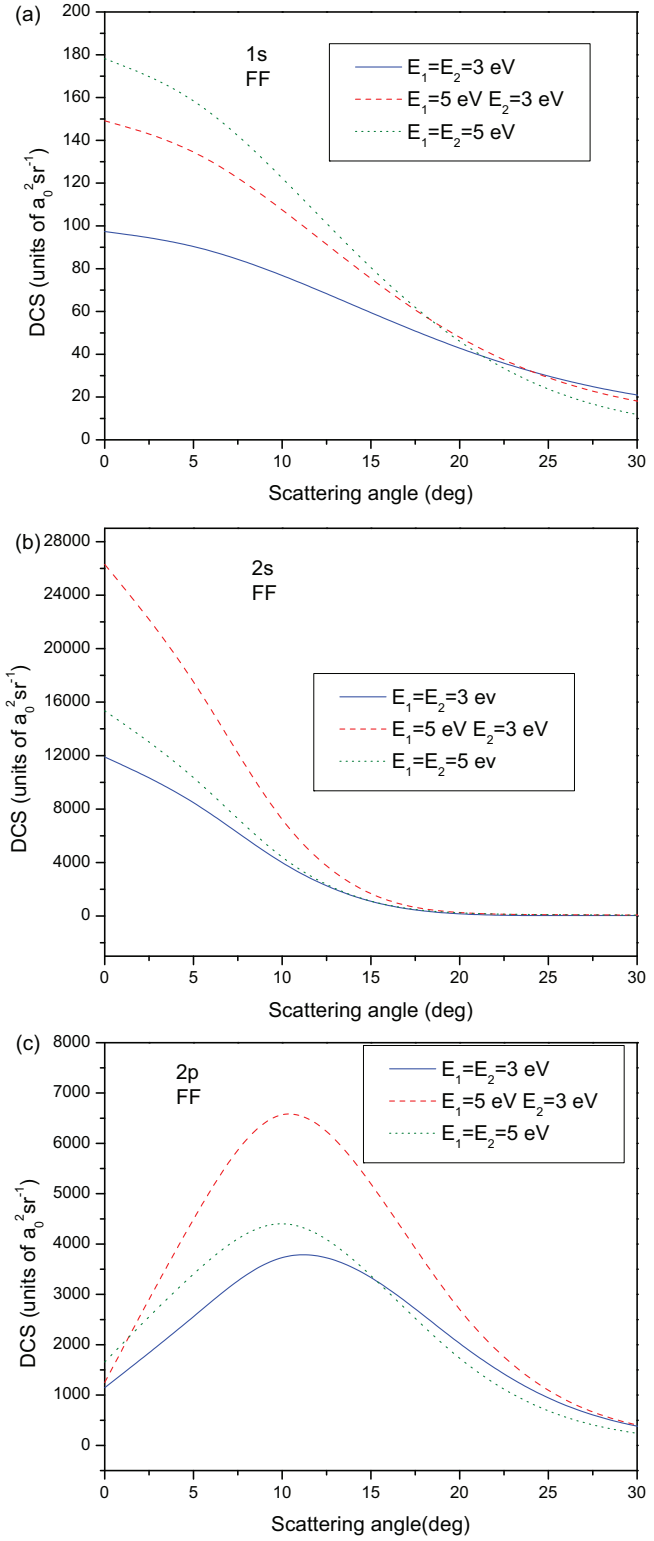


FIG. 1. (Color online) Differential cross sections (DCS) (in $a_0^2$ sr$^{-1}$ units) for antihydrogen formation in (a) $1s$, (b) $2s$, and (c) $2p$ states in antiproton-positron-positron collision for the field-free (FF) situation. The Debye parameter ($\mu$) is chosen as 0.12 and the angle between the active and passive positron is $\theta_1 = 0^\circ$.

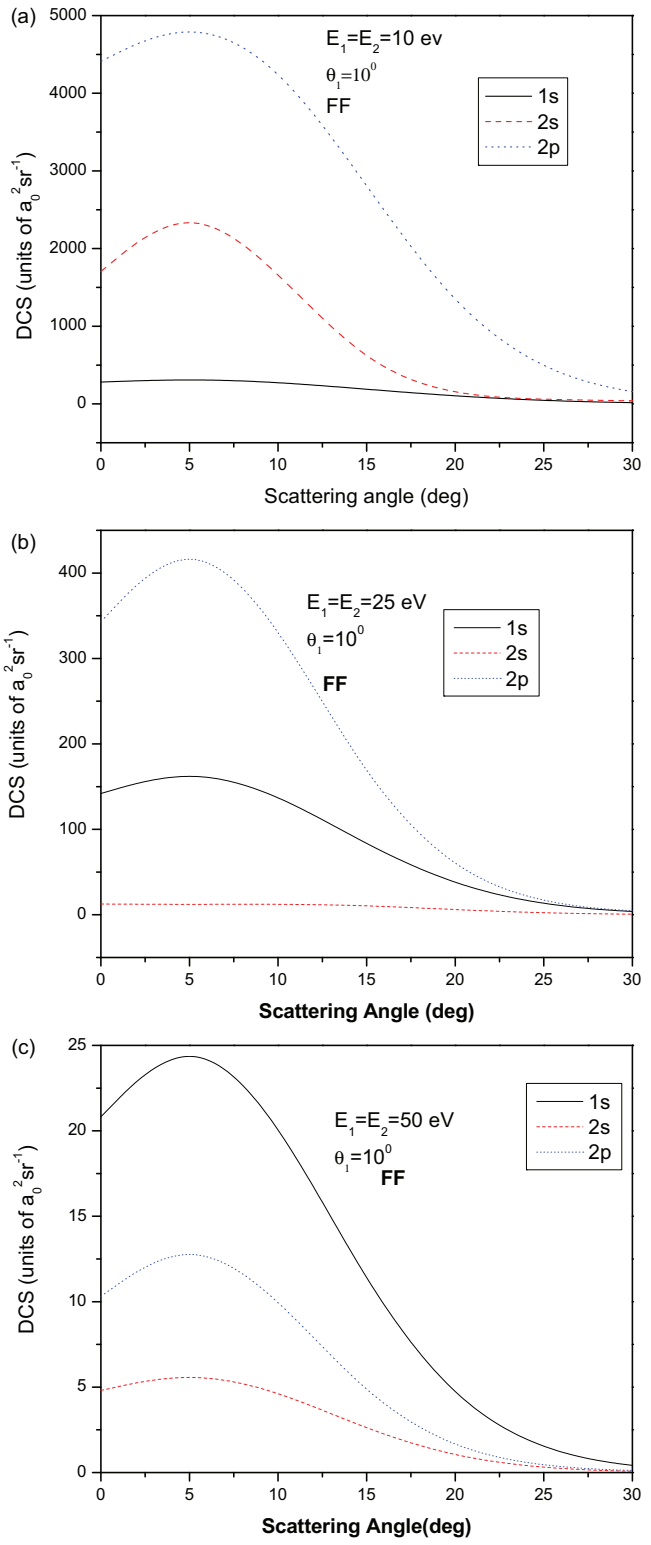


FIG. 2. (Color online) Same DCS as in Fig. 1 for $1s$, $2s$, and $2p$ states but for equal energy sharing between the two incident positrons and $\theta_1$ is chosen to be $10^\circ$, the Debye parameter remaining the same: (a) $E_1 = E_2 = 10$ eV, (b) $E_1 = E_2 = 25$ eV, and (c) $E_1 = E_2 = 50$ eV.

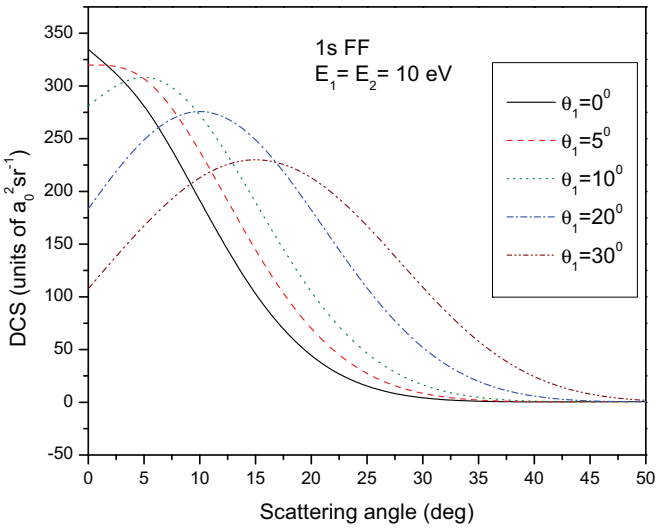


FIG. 3. (Color online) Same DCS as in Fig. 1 for the $1s$ state but for different angles between the active and spectator positrons.

spectator positrons consistently. The laser field strength and the laser frequency are chosen to be $\varepsilon_0 = 5.145 \times 10^8$ V/m and $\omega = 1.17$ eV, respectively. The field polarization is considered to be parallel to the momentum of the passive positron ($\vec{k}_2$), being the polar axis, while $\theta_1$ is the incident angle of the active positron ($\vec{k}_1$).

Figures 1(a)–1(c) exhibit the DCS in the ground and excited states ($2s$ and $2p$) for some equal energy ($E_1 = E_2$) as well as unequal energy ($E_1 \neq E_2$) shared between the two positrons in the FF situation. The figures reveal that the ground state DCS [see Fig. 1(a)] increases with the increase in the sum total energy ($E_1 + E_2$) at lower scattering angles (up to $\sim 25^\circ$), while the excited ($2s$,$2p$) state DCS [see Figs. 1(b) and 1(c)] for unequal energies lie much above those for equal energies. Since in the present model, the two incident positrons are treated on an equal footing, the behavior of the formation cross section is found to be symmetric with respect to the interchange of $E_1$ and $E_2$. For all the energy sets in the Figs 1(a)–1(c), the field-free DCS follows the order $2s > 2p > 1s$. The figures also indicate that for all the states, the formation cross section is strongly favored in the forward direction beyond which ($\sim 30^\circ$) the cross sections die out and become almost negligible, and as such the results are plotted only up to that.

Figures 2(a)–2(c) show similar FF results for the ground and excited states for equal energies ($E_1 = E_2$) of the two positrons. At low incident energy, the magnitude of the $\bar{\mathrm{H}}$ formation cross section is found to be largest for the $2p$ state and smallest for the $1s$ state, while the $2s$ state lies in between, i.e., $2p > 2s > 1s$ [see Fig. 2(a)]. With increasing incident energy, the $2s$ and $2p$ cross sections decrease, while the $1s$ increases. As a result, at intermediate energies, we note $2p > 1s > 2s$ [see Fig. 2(b)] while at higher energies (e.g., 50 eV onwards) the ground state TBR cross sections are found [see Fig. 2(c)] to dominate over the excited states ($2s$,$2p$).

Figure 3 represents only the ground state field-free DCS for $E_1 = E_2$ but with different values of the angle between the two positrons. As noted from the figure, the DCS is quite sensitive with respect to the incident angle ($\theta_1$) of the active positron, e.g., the DCS peak value gradually decreases with the increase in the angle between the positrons, which is expected physically.

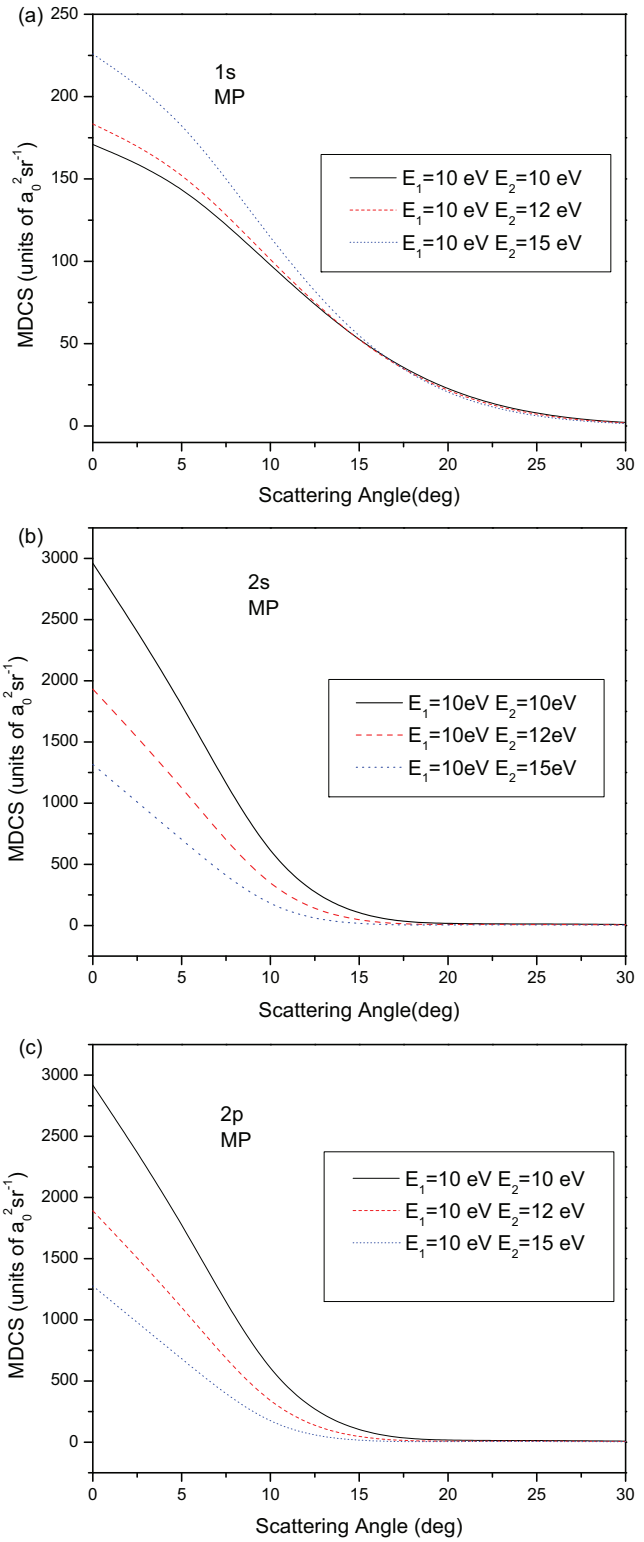


FIG. 4. (Color online) MDCS (in $a_0^2$ sr$^{-1}$ units) for laser-assisted antihydrogen formation in (a) $1s$, (b) $2s$, and (c) $2p$ states for unequal as well as equal energies of the two positrons.

Figures 4(a)–4(c) represent the multiphoton differential cross section (MDCS) in both the ground and excited states for

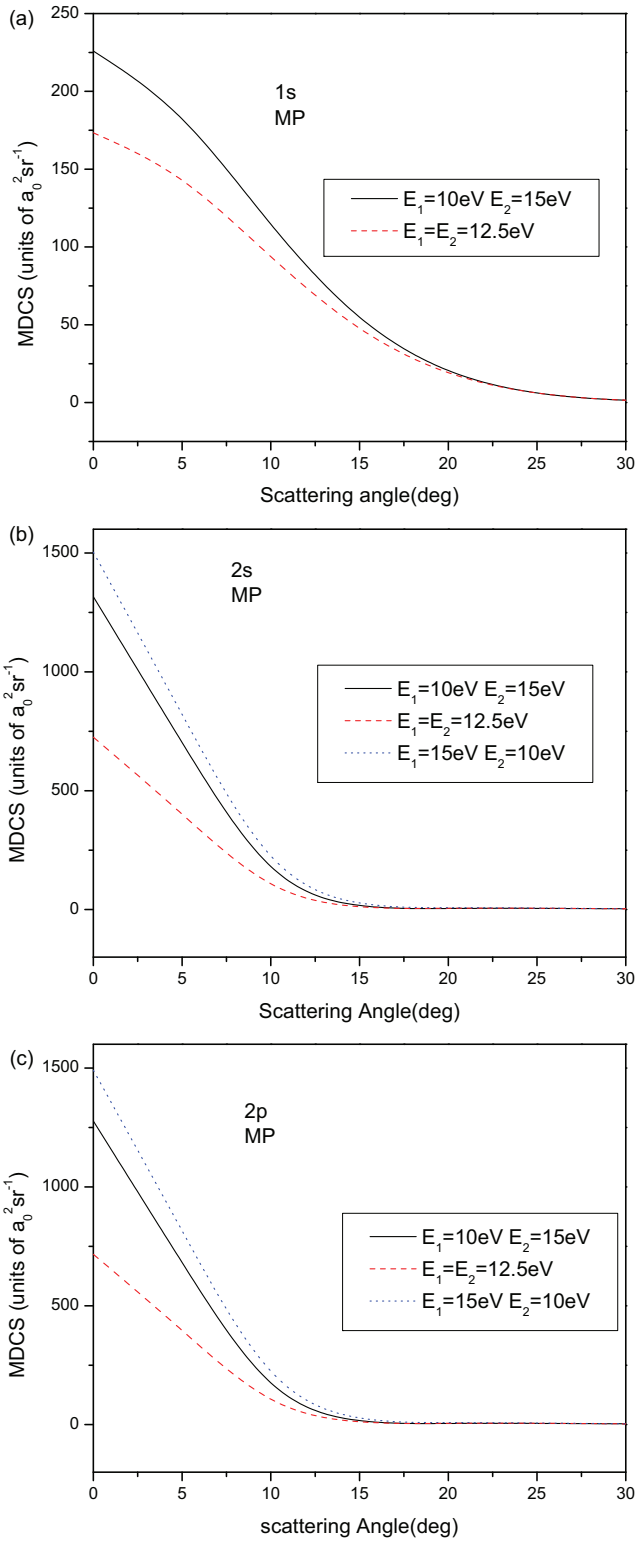


FIG. 5. (Color online) Same MDCS as in Fig. 4 for (a) 1$s$ (b) 2s, and (c) 2$p$ states but for a fixed value of the sum total energy $(E_1 + E_2)$.

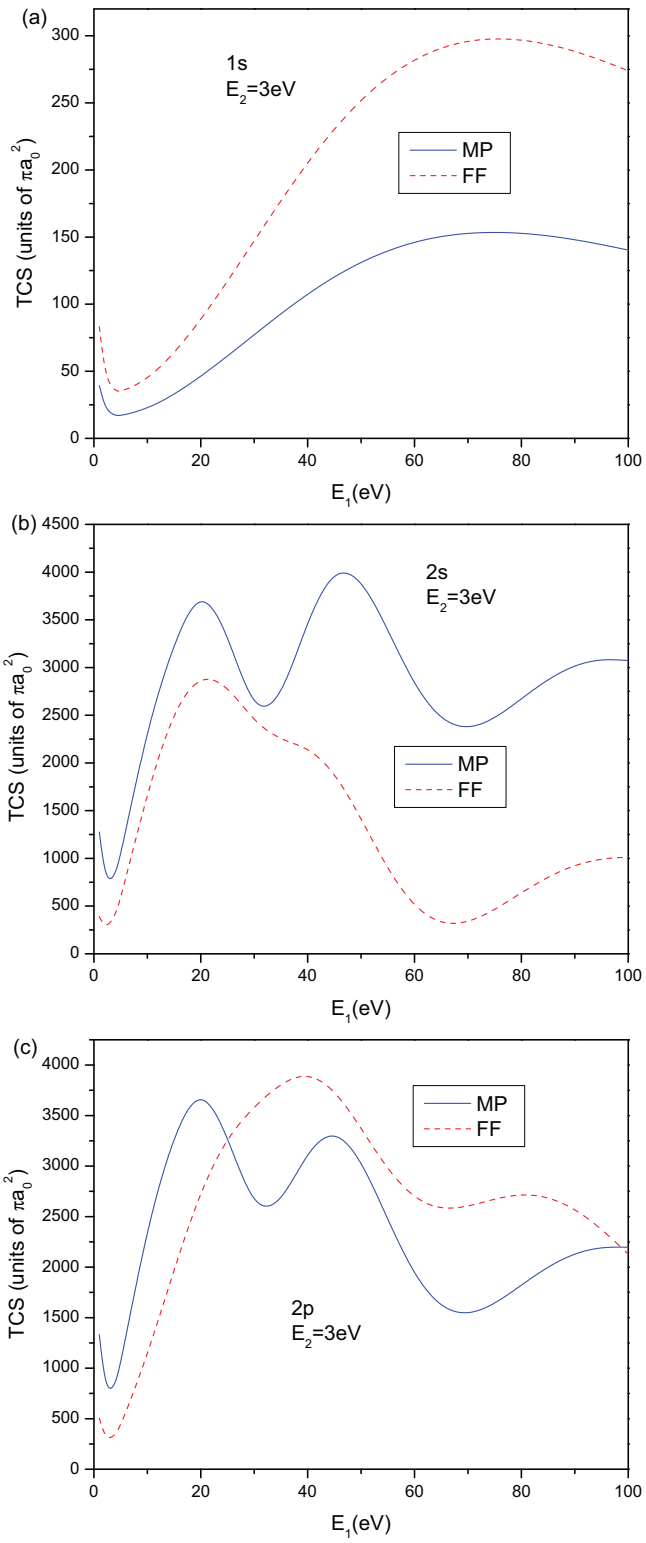


FIG. 6. (Color online) Multiphotontotal cross sections (MTCS) (in units of $\pi a_0^2$) along with field-free TCS in (a) 1$s$, (b) 2$s$, and (c) 2$p$ states against active $e^+$ energy $E_1$ for a fixed value of spectator $e^+$ energy $E_2 = 3$ eV.

some equal $(E_1 = E_2)$ as well as unequal $(E_1 \neq E_2)$ energies of the two positrons. The figures indicate that the ground state MDCS [Fig. 4(a)] is highest for the highest value of the sum of the energies $(E_1 + E_2)$ and lowest for the lowest value of the same. In contrast, for the excited states (2$s$,2$p$) it is just the reverse, i.e., the MDCS is maximum for a minimum value of $(E_1 + E_2)$ and vice versa [Figs. 4(b) and 4(c)].

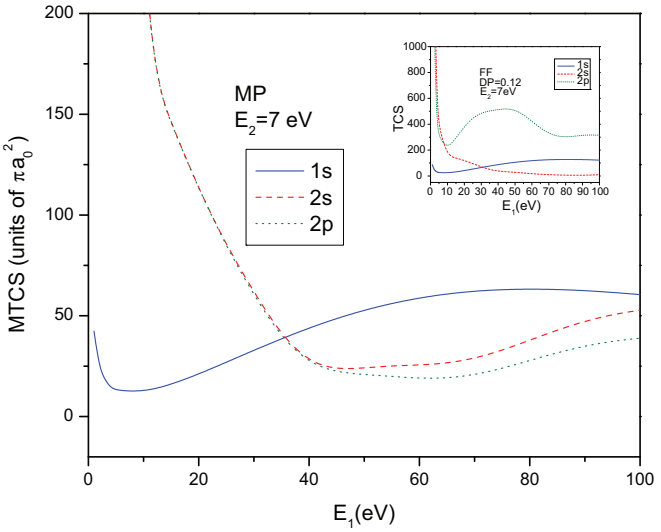


FIG. 7. (Color online) Multiphoton total cross sections (MTCS) (in units of $\pi a_0^2$) for laser-assisted antihydrogen formation in $1s$, $2s$, and $2p$ states against active $e^+$ energy $E_1$ for a fixed value of spectator $e^+$ energy $E_2 = 7$ eV. Inset: same TCS but in the FF case.

Figures 5(a)–5(c) represent the same MDCS but for a fixed value of $(E_1 + E_2)$. We find that the ground state MDCS [Fig. 5(a)] is higher for the unequal energy $(E_1 \neq E_2)$ case than for the equal $(E_1 = E_2)$ one. Further, it is interesting to note that unlike the FF case, the multiphoton DCS for the excited states [Figs. 5(b) and 5(c)] loses the symmetric nature with respect to $E_1$ and $E_2$, e.g., the MDCS for $2s$ and $2p$ follow the order $(E_1 > E_2) > (E_1 < E_2) > (E_1 = E_2)$, while in contrast, the ground state MDCS retains its FF symmetric nature.

Now we turn to the multiphoton total cross section (MTCS) for the $\bar{\mathrm{H}}$ formation for ground and excited $(n = 2)$ states against the active positron energy $(E_1)$ for a fixed value of the spectator energy $E_2$. Figures 6(a)–6(c) clearly demonstrate the effect of multiphoton exchange as compared to the FF case, e.g., the ground state TCS is suppressed (as compared to the FF), while the $2s$ state TCS is enhanced throughout the energy range; the degree of suppression or enhancement is higher for the higher energy range (>50 eV). On the other hand, the $2p$ cross section is enhanced up to a certain value of $E_1$ (depending on $E_2$) beyond which it is suppressed as compared to the FF results.

Figure 7 exhibits a comparison between the $1s$, $2s$, and $2p$ MTCS against $E_1$ for a fixed value of $E_2 = 7$ eV. At very low $E_1$ (0–5 eV), the MTCS follows the order $2p > 2s > 1s$, while in the FF case (see inset) the order is $2s > 2p > 1s$. In the intermediate energies (5 eV $< E_1 <$ 35 eV), the MTCS order is $2s >$ 2p $> 1s$, unlike the FF order $2p > 2s > 1s$. However, at higher values of $E_1$ (>35 eV), the ground state MTCS dominates with the order $1s > 2s > 2p$ in contrast to the FF case $2p > 1s > 2s$ (see inset), indicating the importance of the multiphoton effect on the ground state to enhance the formation cross sections with respect to the FF case in this energy region.

Figures 8(a)–8(c) show the variation of MTCS with respect to $E_1$ in the ground and excited states for different values of the spectator energy $E_2$. The figures reveal that at low

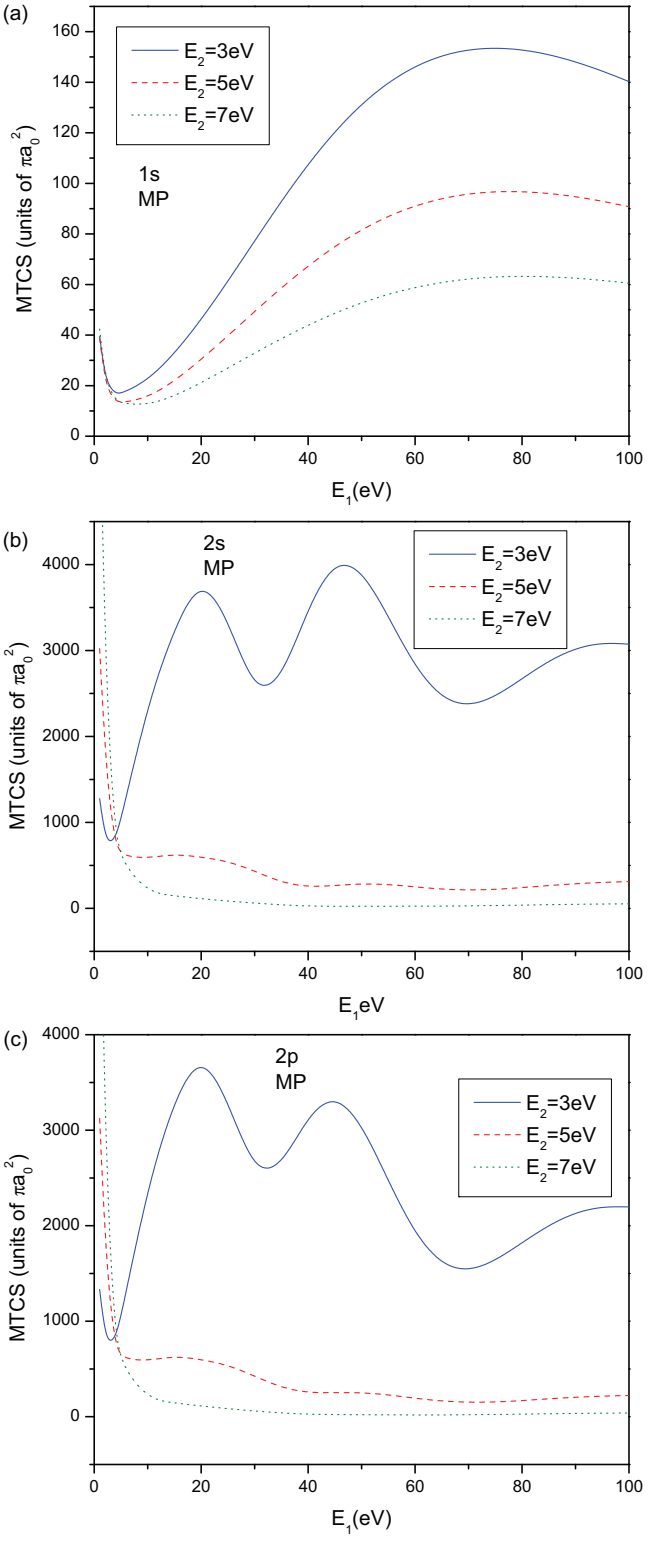


FIG. 8. (Color online) Multiphoton total cross sections (MTCS) (in units of $\pi a_0^2$) for laser-assisted antihydrogen formation in (a) $1s$, (b) $2s$, and (c) $2p$ states against active $e^+$ energy $E_1$ for different values of spectator $e^+$ energy $E_2$.

$E_1$ (0–5 eV), the MTCS increases with increasing $E_2$, while beyond 5 eV, the MTCS increases with decreasing $E_2$ for all the states ($1s$,$2s$,$2p$). It is also evident from the figures that

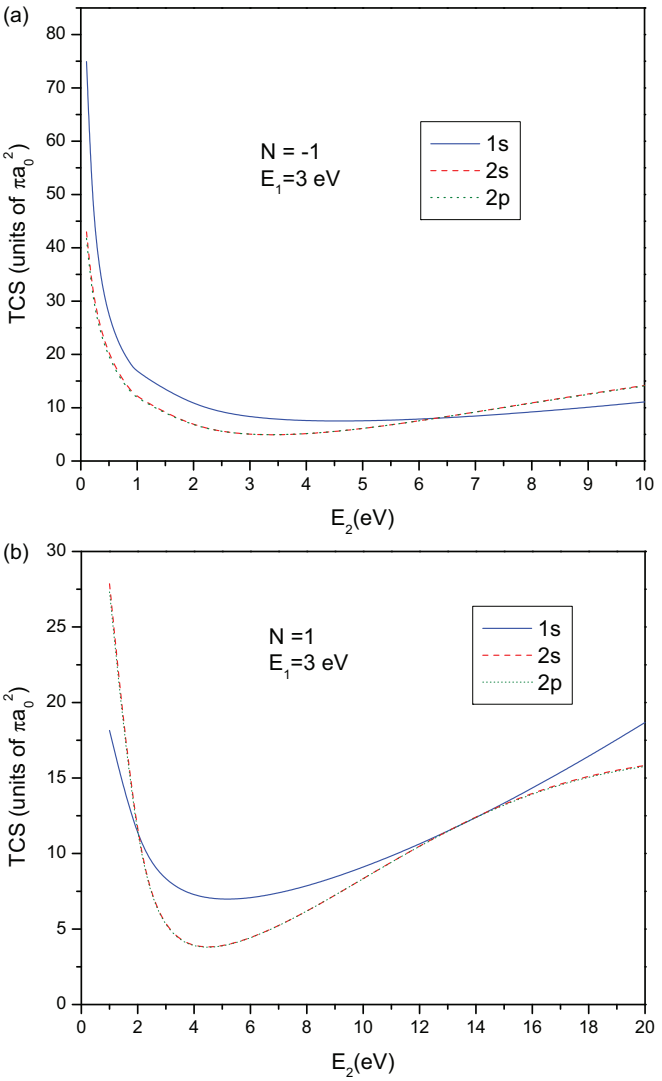


FIG. 9. (Color online) Single-photon TCS (in units of $\pi a_0^2$) for laser-assisted antihydrogen formation against spectator $e^+$ energy $E_2$ for a fixed value of active $e^+$ energy $E_1 = 3$ eV. (a) Single-photon emission ($N = -1$) TCS. (b) Single-photon absorption ($N = +1$) TCS.

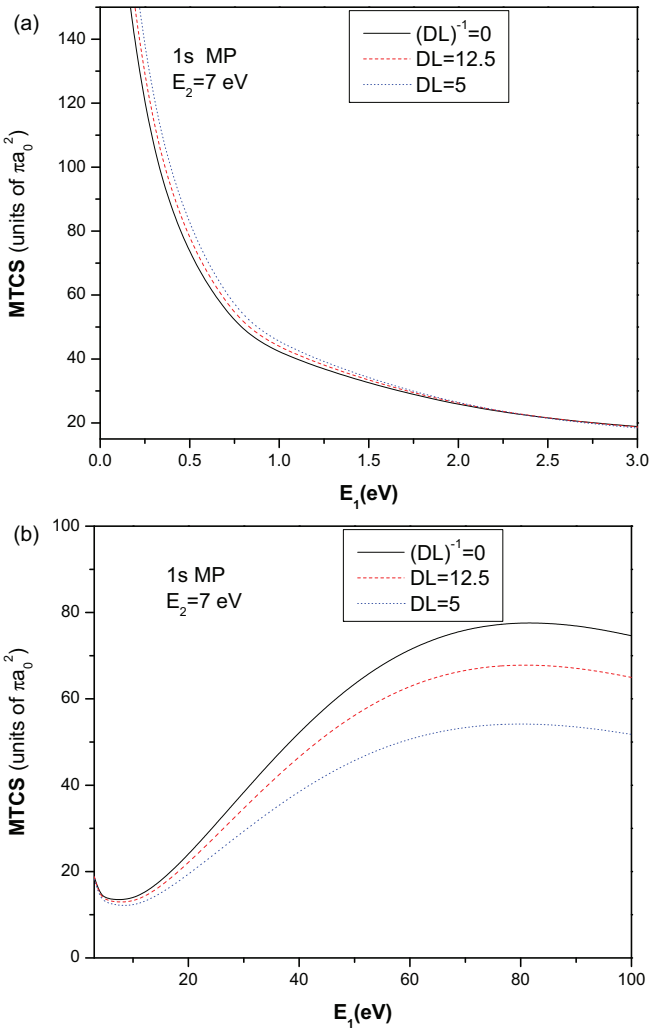


FIG. 10. (Color online) Multiphoton total cross sections (MTCS) (in units of $\pi a_0^2$) for laser-assisted antihydrogen formation against active $e^+$ energy $E_1$ for a fixed value of spectator $e^+$ energy $E_2 = 7$ eV in the $1s$ state. (a) $E_1 < 3$ eV and (b) $E_1 > 3$ eV.

the formation cross section is higher for a higher value of the energy difference between the active ($E_1$) and the spectator ($E_2$) positrons. This is quite expected physically due to less repulsion between the positrons for higher values of the energy difference.

Figures 9(a) and 9(b) display single-photon ($N = \pm 1$) absorption and emission TCS against $E_2$, keeping $E_1$ fixed at 3 eV. Figure 9(a) indicates an important inference that at low energy regime, the ground state single-photon emission ($N = -1$) TCS is higher than that of the excited states. This finding has a great implication since for high precision spectroscopic studies the ground state is essential and is the main concern of the $\bar{\text{H}}$ experiments at CERN. Thus to obtain higher ground state formation cross sections (than the excited ones) at lower incident energies, a weak laser field could be suggested.

Figures 10(a) and 10(b) show the variation of ground state MTCS with respect to the Debye length ($\Lambda$). It is important to note that at low $E_1$ (up to $\sim$3 eV), the formation cross section (MTCS) is higher for higher values of the Debye screening ($\mu$), i.e., for lower Debye length [Fig. 10(a)], while beyond 3 eV, the MTCS becomes lower for higher Debye screening [see Fig. 10(b)]. On the contrary, the MTCS for the excited states increases with the decrease in $\mu$ up to $E_1 \sim 15$ eV beyond which it becomes almost insensitive with respect to the variation of $\mu$ (not shown in the figure). Similar behavior is noted for the equal energy case ($E_1 = E_2$; not shown). Thus, another way to enhance the ground state MTCS in the low energy region is to use a higher value of the Debye screening $\mu$ or a lower value of $\Lambda$.

Figures 11(a) and 11(b) exhibit the MTCS for equal energy sharing $E_1 = E_2$ along with the corresponding FF results. The excited state TCS in both the FF and LA situations exhibit a distinct peak at $\sim$3 eV beyond which it decreases sharply, whereas the ground state TCS gradually decreases up to a certain energy [$\sim$5 eV; Fig. 11(a), inset] after which it becomes almost an asymptote.

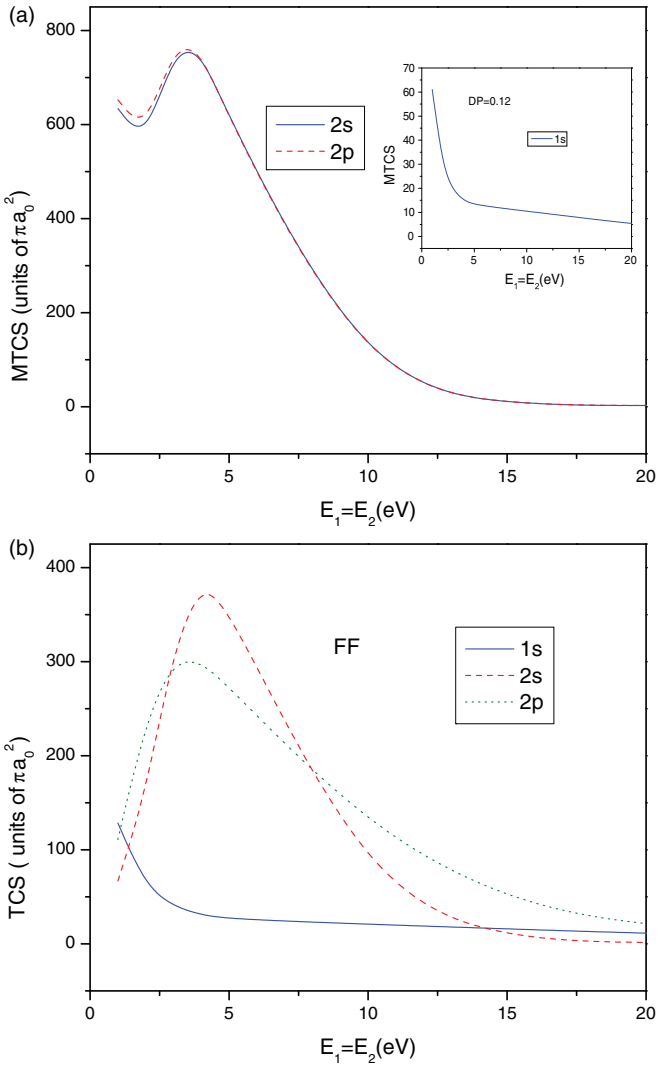


FIG. 11. (Color online) (a) Multiphoton total cross sections (MTCS) (in units of $\pi a_0^2$)for laser-assisted antihydrogen formation for equal energy sharing ($E_1 = E_2$) between the two incident $e^+$'s in excited ($2s$,$2p$) states. Inset: same MTCS for the $1s$ state. (b) Same TCS in the FF situation.

Figures 12(a)–12(c) illustrate the distribution of the partial TCS among the different multiphoton processes at some fixed values of the incident energies of the two positrons. As revealed from the figures, the ground state TCS is minimum for the zero photon exchange ($N = 0$) and is much lower than the higher photon exchange. In contrast, the excited states TCS are maximum for the zero photon exchange and are much lower for the higher photon exchange than for the zero photon one. For a given value of $N$, the emission cross sections are in general much higher than the absorption ones, which is expected for an exothermic reaction.

Table I displays a numerical measure of the single-photon ($N = \pm 1$), multiphoton, as well as the FF total cross sections with respect to active positron energy $E_1$ for a fixed value of the passive positron energy, $E_2 = 7$ eV. The most important inferences that can be drawn from Table I are as follows: (1) the single-photon TCS for the excited states are suppressed throughout with respect to the FF, while the ground state TCS

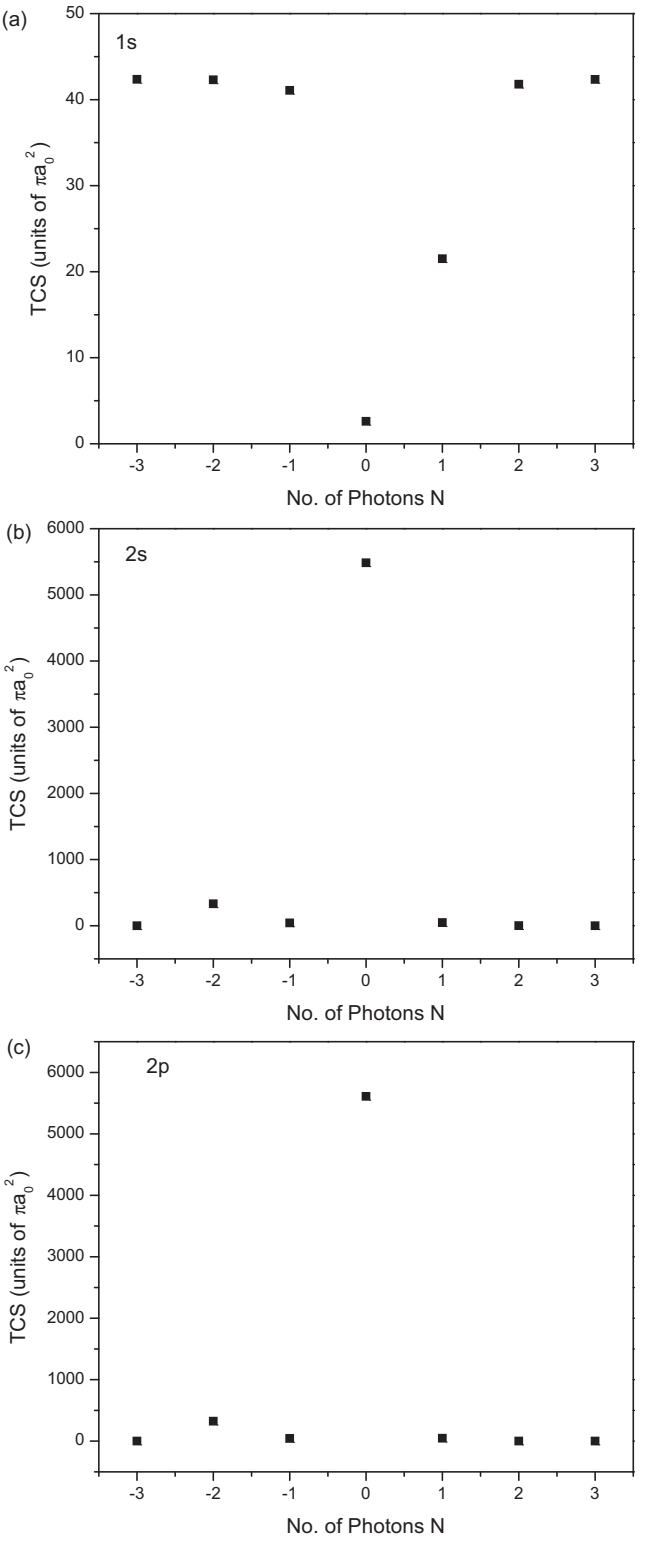


FIG. 12. (a) Total cross section (in units of $\pi a_0^2$) vs the number of photons emitted or absorbed in the ground state for $E_1$ (active $e^+$ energy) = 1 eV, $E_2$ (spectator $e^+$ energy) = 7 eV. (b) Same TCS for the $2s$ state. (c) Same TCS for the $2p$ state.

is suppressed up to a value of $E_1 \sim 10$ eV (depending on $E_2$) and then starts to enhance, and (2) the multiphoton ground state cross section gradually increases with increasing values

TABLE I. Laser-assisted $\bar{H}$ formation cross section (for single as well as multiphoton exchange) for a fixed value of $E_2 = 7$ eV along with corresponding field-free TCS for the laser field strength $\varepsilon_0 = 5.14 \times 10^8$ V/m and the photon energy $\hbar\omega$ =1.17 eV.

| $E_1$ | Absorption | | | Emission | | | FF TCS / MTCS | | |
|---|---|---|---|---|---|---|---|---|---|
| (eV) | $N = +1$ TCS | | | $N = -1$ TCS | | | | | |
| | $1s$ | $2s$ | $2p$ | $1s$ | $2s$ | $2p$ | $1s$ | $2s$ | $2p$ |
| 1 | 18.8 | 47.6 | 47.1 | 19.5 | 42.8 | 42.8 | 87.9 | 3576.4 | 3416.2 |
| | | | | | | | 42.3 | 5910.6 | 6025.1 |
| 2 | 10.3 | 11.4 | 11.3 | 11.3 | 17.2 | 17.2 | 49.9 | 1843.9 | 1294.7 |
| | | | | | | | 24.3 | 3184.4 | 3204.5 |
| 3 | 7.37 | 5.20 | 5.20 | 8.42 | 9.18 | 9.17 | 36.0 | 995.6 | 663.3 |
| | | | | | | | 18.2 | 1675.5 | 1671.1 |
| 4 | 6.02 | 3.48 | 3.47 | 7.03 | 5.49 | 5.44 | 29.3 | 573.5 | 409.6 |
| | | | | | | | 14.6 | 917.4 | 910.0 |
| 5 | 5.31 | 2.73 | 2.71 | 6.25 | 3.66 | 3.60 | 25.8 | 362.9 | 291.4 |
| | | | | | | | 12.9 | 546.9 | 541.1 |
| 10 | 5.15 | 1.99 | 1.97 | 6.15 | 1.93 | 1.91 | 24.0 | 154.6 | 209.7 |
| | | | | | | | 12.2 | 182.1 | 181.5 |
| 15 | 6.77 | 2.07 | 2.06 | 8.28 | 1.83 | 1.82 | 31.2 | 139.1 | 293.3 |
| | | | | | | | 15.8 | 145.6 | 145.4 |
| 20 | 9.01 | 1.95 | 1.94 | 11.2 | 1.60 | 1.58 | 41.6 | 119.0 | 381.4 |
| | | | | | | | 21.1 | 112.8 | 112.8 |
| 25 | 11.4 | 1.68 | 1.67 | 14.4 | 1.16 | 1.16 | 53.2 | 95.4 | 449.6 |
| | | | | | | | 26.9 | 85.0 | 84.5 |
| 30 | 13.9 | 1.38 | 1.37 | 17.6 | 0.88 | 0.90 | 65.2 | 70.2 | 487.8 |
| | | | | | | | 32.9 | 61.8 | 60.2 |
| 35 | 16.3 | 1.08 | 1.06 | 20.7 | 0.93 | 0.89 | 76.7 | 49.0 | 503.1 |
| | | | | | | | 38.6 | 40.3 | 39.2 |
| 40 | 18.6 | 0.81 | 0.80 | 23.6 | 0.87 | 0.79 | 87.5 | 37.4 | 513.8 |
| | | | | | | | 43.9 | 27.0 | 26.5 |
| 50 | 22.3 | 0.54 | 0.54 | 28.2 | 0.30 | 0.29 | 105.6 | 28.2 | 510.2 |
| | | | | | | | 52.7 | 24.1 | 20.8 |
| 60 | 24.9 | 0.41 | 0.39 | 31.2 | 0.62 | 0.58 | 118.2 | 17.2 | 423.0 |
| | | | | | | | 58.8 | 25.5 | 18.9 |
| 80 | 27.0 | 0.27 | 0.23 | 33.1 | 1.24 | 0.95 | 127.6 | 5.7 | 302.0 |
| | | | | | | | 63.2 | 37.8 | 27.8 |
| 100 | 26.0 | 0.53 | 0.46 | 31.1 | 0.81 | 0.67 | 122.3 | 9.4 | 314.3 |
| | | | | | | | 60.4 | 52.8 | 38.9 |

of $E_1$ and beyond ∼35 eV it dominates over the excited state cross sections.

Table II displays the same numerical measure as in Table I but for equal energies ($E_1 = E_2$) of the two positrons. The most important findings from Table II are noted below.

(1) The single-photon TCS for both ground and excited states decrease with increasing energies and become negligible beyond ∼30 eV. (2) The ground state single-photon emission ($N = -1$) TCS dominates over the excited states throughout the energies, while the single-photon absorption ($N = +1$) TCS follow the order 2s > $2p$ > $1s$ at very low energies (up to ∼2 eV) and beyond that the ground state dominates over the excited ones throughout. (3) The multiphoton TCS for the ground state is suppressed with respect to the FF ones throughout the energies, while the $2p$ state MTCS is enhanced up to energy ∼7 eV and beyond that it is suppressed as compared to the FF one. However, the $2s$ state MTCS shows an exceptional behavior, e.g., it is enhanced up to $E \sim 9$ eV, then gets suppressed up to $E \sim 15$ eV and again is enhanced beyond 15 eV with respect to the FF ones. (4) Up to $E \sim 12$ eV, the MTCS follow the order $2s > 2p > 1s$, while beyond 13 eV the ground state MTCS dominates over the excited ones.

## IV. CONCLUSION

The most salient features of the present study are as follows. At very low incident energies, the field-free TBR cross section for the $\bar{H}$ formation in the $2s$ state is found to be dominant among the three states and the TCS follow the order $2s > 2p > 1s$ for unequal energy sharing ($E_1 \neq E_2$) between the incident positrons. At intermediate energies, the order for the FF TCS is $2p > 2s > 1s$, while at higher incident energies, the ground state dominates over the $2s$ state but the $2p$ remains the maximum ($2p > 1s > 2s$). However, for

TABLE II. Laser-assisted $\bar{H}$ formation cross sections (for single as well as for multiphoton exchange) for different sets of equal energy ($E_1 = E_2$) along with the corresponding field-free TCS for the laser field with field strength $\varepsilon_0 = 5.14 \times 10^8$ V/m and the photon energy 1.17 eV.

| Incident energy (eV) | $N = +1$ TCS | | | $N = -1$ TCS | | | FF TCS/MTCS | | |
|---|---|---|---|---|---|---|---|---|---|
| | $1s$ | $2s$ | $2p$ | $1s$ | $2s$ | $2p$ | $1s$ | $2s$ | $2p$ |
| 1 | 29.5 | 42.9 | 42.6 | 24.8 | 9.72 | 9.67 | 128.4 | 66.7 | 110.9 |
| | | | | | | | 61.0 | 634.0 | 652.8 |
| 2 | 12.9 | 13.7 | 13.5 | 11.9 | 6.95 | 6.94 | 61.0 | 160.0 | 236.5 |
| | | | | | | | 28.8 | 558.1 | 578.8 |
| 3 | 8.08 | 4.80 | 4.75 | 8.17 | 4.77 | 4.76 | 39.8 | 313.9 | 302.5 |
| | | | | | | | 19.0 | 761.2 | 771.6 |
| 4 | 6.16 | 2.65 | 2.64 | 6.62 | 4.13 | 4.12 | 30.7 | 385.6 | 300.4 |
| | | | | | | | 14.9 | 760.1 | 761.2 |
| 5 | 5.38 | 2.42 | 2.40 | 6.04 | 3.67 | 3.64 | 26.4 | 358.6 | 272.8 |
| | | | | | | | 13.1 | 606.8 | 604.1 |
| 6 | 4.91 | 2.31 | 2.30 | 5.82 | 3.02 | 2.91 | 24.2 | 283.6 | 239.9 |
| | | | | | | | 12.1 | 423.3 | 420.2 |
| 7 | 4.82 | 2.11 | 2.09 | 5.70 | 2.21 | 2.20 | 23.0 | 203.1 | 207.2 |
| | | | | | | | 11.6 | 271.3 | 268.9 |
| 8 | 4.73 | 1.72 | 1.70 | 5.65 | 1.62 | 1.59 | 22.2 | 136.5 | 176.2 |
| | | | | | | | 11.2 | 164.2 | 162.5 |
| 9 | 4.61 | 1.30 | 1.29 | 5.43 | 1.09 | 1.08 | 21.5 | 87.7 | 147.9 |
| | | | | | | | 10.9 | 95.1 | 94.1 |
| 10 | 4.52 | 0.93 | 0.92 | 5.31 | 0.72 | 0.71 | 20.8 | 54.6 | 122.8 |
| | | | | | | | 10.5 | 53.2 | 52.7 |
| 11 | 4.38 | 0.67 | 0.66 | 5.04 | 0.48 | 0.47 | 19.9 | 33.1 | 101.2 |
| | | | | | | | 10.0 | 28.9 | 28.7 |
| 12 | 4.26 | 0.46 | 0.45 | 4.82 | 0.32 | 0.31 | 19.0 | 19.6 | 82.8 |
| | | | | | | | 9.5 | 15.4 | 15.3 |
| 13 | 3.91 | 0.28 | 0.27 | 4.50 | 0.24 | 0.24 | 18.0 | 11.4 | 67.6 |
| | | | | | | | 8.92 | 8.21 | 8.20 |
| 14 | 3.78 | 0.22 | 0.21 | 4.21 | 0.19 | 0.19 | 17.0 | 6.5 | 55.1 |
| | | | | | | | 8.44 | 4.71 | 4.70 |
| 15 | 3.53 | 0.15 | 0.14 | 3.93 | 0.13 | 0.13 | 15.9 | 3.7 | 44.8 |
| | | | | | | | 7.83 | 3.06 | 3.12 |
| 20 | 2.30 | 0.08 | 0.08 | 2.51 | 0.11 | 0.11 | 10.9 | 0.8 | 16.4 |
| | | | | | | | 5.34 | 2.55 | 2.67 |
| 30 | 0.93 | 0.07 | 0.07 | 0.97 | 0.08 | 0.08 | 4.61 | 0.8 | 2.7 |
| | | | | | | | 2.21 | 1.73 | 1.74 |

equal energies ($E_1 = E_2$), the $2p$ state dominates for low and intermediate energies, while the ground state is maximum for high incident energies.

Since in the present model the incident positrons are treated on an equal footing the FF cross section is symmetric with respect to $E_1$ and $E_2$ for both the ground and the excited ($2s$,$2p$) states, unlike the field-assisted case where only the ground state is symmetric but not the excited ones.

The ground state single-photon emission ($N = -1$) TCS is dominant over the excited states in the low energy regime (∼0–6 eV) indicating that a weaker field is favored for enhanced formation of ground state $\bar{H}$ at low incident energies. This might have important implications in the context of high precision spectroscopic studies.

On the other hand, for single-photon absorption ($N = +1$), the ground state TCS dominates over the excited ones beyond a low $E_1$ (∼2 eV) depending on the value of $E_2$ while in contrast, the ground state multiphoton TCS dominates beyond a higher value of $E_1$ (∼35 eV). However, for equal energy ($E_1 = E_2$), the ground state multiphoton TCS dominates over the excited states ($2s$,$2p$) beyond the incident energy ∼10–15 eV. At low incident energies, the ground state MTCS can be enhanced

with higher Debye screening $\mu$, while the excited state MTCS enhances for lower $\mu$.

For the experimental extreme low energies ($\sim$meV range), the present model is not supposed to be suitable and a more sophisticated theory is needed. Finally, the present findings (both FF and LA) might give some physical insight to future detailed antihydrogen formation experiments.


[1] C. Zimmerman and T. W. Hansch, Nucl. Phys. A **558**, 625c (1993).
[2] R. G. Greaves and C. M. Surko, Phys. Plasmas **4**, 1528 (1997).
[3] M. H. Holzscheiter and M. Charlton, Rep. Prog. Phys. **62**, 1 (1999).
[4] G. Gabrielse, J. Estrada, J. N. Tan, P. Yesley, N. S. Bowden, P. Oxley, T. Roach, C. H. Storry, M. Wessels *et al.*, Phys. Lett. B **507**, 1 (2001).
[5] M. Amoretti *et al.*, Nature (London) **419**, 456 (2002); Phys. Lett. B **583**, 59 (2004).
[6] G. Gabrielse *et al.*, Phys. Rev. Lett. **89**, 213401 (2002).
[7] A. Speck, C. H. Storry, E. A. Hessels, and G. Gabrielse, Phys. Lett. B **597**, 257 (2004).
[8] C. H. Storry *et al.*, Phys. Rev. Lett. **93**, 263401 (2004).
[9] G. Gabrielse, Adv. At. Mol. Opt. Phys. **50**, 155 (2005).
[10] M. Amoretti *et al.*, Phys. Rev. Lett. **97**, 213401 (2006).
[11] T. Pohl, H. R. Sadeghpour, and G. Gabrielse, Phys. Rev. Lett. **97**, 143401 (2006); T. Pohl, H. R. Sadeghpour, and P. Schmelcher, Phys. Rep. **484**, 181 (2009).
[12] G. B. Andresen *et al.*, Phys. Rev. Lett. **98**, 023402 (2007).
[13] G. Gabrielse *et al.*, Phys. Rev. Lett. **98**, 113002 (2007).
[14] M. C. Fujiwara *et al.*, Phys. Rev. Lett. **101**, 053401 (2008).
[15] G. Gabrielse *et al.*, Phys. Rev. Lett. **100**, 113001 (2008).
[16] G. B. Andresen *et al.*, J. Phys. B **41**, 011001 (2008).
[17] G. B. Andresen *et al.*, Phys. Rev. Lett. **100**, 203401 (2008).
[18] G. B. Andresen *et al.*, Phys. Plasmas **16**, 100702 (2009).
[19] G. B. Andresen *et al.*, Nature (London) **468**, 673 (2010).
[20] G. B. Andresen *et al.*, Phys. Lett. B **685**, 141 (2010).
[21] N. Masden, Philos. Trans. R. Soc. London, Ser. A **368**, 3671 (2010).
[22] G. B. Andresen *et al.*, Nat. Phys. **7**, 558 (2011).
[23] G. B. Andresen *et al.*, Phys. Lett. B **695**, 95 (2011).
[24] C. Amole *et al.*, New J. Phys. **14**, 105010 (2012).
[25] C. Amole *et al.*, Nature (London) **483**, 439 (2012).
[26] G. B. Andresen *et al.*, Nucl. Instrum. Methods Phys. Res. A **684**, 73 (2012).
[27] G. Gabrielse *et al.*, Phys. Rev. Lett. **108**, 113002 (2012).
[28] B. Juhasz, Hyperfine Interact. **212**, 69 (2012).
[29] C. Amole *et al.*, Phys. Plasmas **20**, 043510 (2013).
[30] The ALPHA Collaboration and A. E. Charman, Nat. Commun. **4**, 1785 (2013).
[31] M. E. Glinsky and T. M. O'Neil, Phys. Fluids B **3**, 1279 (1991).
[32] F. Robicheaux, J. Phys. B **40**, 271 (2007).
[33] F. Robicheaux, J. Phys. B **41**, 192001 (2008).
[34] E. M. Bass and D. H. E. Dubin, Phys. Plasmas **16**, 012101 (2009).
[35] S. Roy, S. Ghosh Deb, and C. Sinha, Phys. Rev. A **78**, 022706 (2008).
[36] S. Ghosh Deb and C. Sinha, Europhys. Lett. **88**, 23001 (2009).
[37] S. M. Li, Z. J. Chen, Q. Q. Wang, and Z. F. Zhou, Eur. Phys. J. D **7**, 39 (1999).
[38] S. M. Li, Z. J. Chen, Z. F. Zhou, and Q. Q. Wang, Phys. Rev. A **59**, 1697 (1999).
[39] S. M. Li, A. H. Liu, Z. F. Zhou, and J. J. Chen, J. Phys. B **33**, 4627 (2000).
[40] R. J. Whitehead, J. F. McCann, and I. Shimamura, Phys. Rev. A **64**, 023401 (2001).
[41] J. S. Cohen, Phys. Rev. A **67**, 017401 (2003).
[42] A. B. Voitkiv, B. Najjari, and J. J. Ullrich, J. Phys. B **35**, 2205 (2002).
[43] J. Mitroy and A. T. Stelbovics, Phys. Rev. Lett. **72**, 3495 (1994).
[44] J. Mitroy and G. J. Ryzhikh, J. Phys. B **30**, L371 (1997).
[45] A. Chattopadhyay and C. Sinha, Phys. Rev. A **74**, 022501 (2006).
[46] B. Zygelman, J. Phys. B **36**, L31 (2003).
[47] M. B. S. Lima, C. A. S. Lima, and L. C. M. Miranda, Phys. Rev. A **19**, 1796 (1979).
[48] G. J. Hatton, N. F. Lane, and J. C. Weisheit, J. Phys. B **14**, 4879 (1981).
[49] N. C. Deb and N. C. Sil, J. Phys. B **17**, 3587 (1984).
[50] B. L. Whitten, N. F. Lane, and J. C. Weisheit, Phys. Rev. A **29**, 945 (1984).
[51] R. S. Pundir and K. C. Mathur, J. Phys. B **17**, 4245 (1984).
[52] J. C. Weisheit, Adv. At. Mol. Phys. **25**, 101 (1988).
[53] B. N. Chichikov, J. Phys. B **23**, L103 (1990).
[54] Z. Q. Wu, G. X. Han, J. Yan, and J. Q. Pang, J. Phys. B **35**, 2305 (2002).
[55] S. Sahoo and Y. K. Ho, Phys. Plasmas **13**, 063301 (2006).
[56] C. Sinha and A. Chattopadhyay, J. Plasma Fusion Res. **7**, 256 (2006).
[57] A. Chattopadhyay and C. Sinha, J. Plasma Fusion Res. **7**, 286 (2006).
[58] S. Chakraborty and Y. K. Ho, Phys. Rev. A **77**, 014502 (2008).
[59] A. Basu and A. S. Ghosh, Nucl. Instrum. Methods Phys. Res. B **266**, 522 (2008).
[60] A. Ghoshal and Y. K. Ho, Eur. Phys. J. D **55**, 581 (2009).
[61] S. Paul and Y. K. Ho, Phys. Plasmas **17**, 082704 (2010).
[62] Y. Chen, Phys. Rev. A **84**, 043423 (2011).
[63] M. C. Zammit, D. V. Fursa, I. Bray, and R. K. Janev, Phys. Rev. A **84**, 052705 (2011).
[64] Arijit Ghoshal and Y. K. Ho, Phys. Scr. **83**, 065301 (2011).
[65] A. K. Bhatia and C. Sinha, Phys. Rev. A **86**, 053421 (2012).
[66] M. C. Zammit, D. V. Fursa, and I. Bray, Chem. Phys. **398**, 214 (2012).
[67] F. Brunel, Phys. Rev. Lett. **59**, 52 (1987).
[68] P. Debye and E. Hückel, Phys. Z. **24**, 185 (1923).
[69] S. Ichimaru, Rev. Mod. Phys. **54**, 1017 (1982).
[70] D. M. Volkov, Z. Phys. **94**, 250 (1935).
[71] G. N. Watson, *A Treatise on the Theory of Bessels Function*, 2nd ed. (Cambridge University Press, Cambridge, England, 1944).